Journal of Volcanology and Geothermal Research 416 (2021) 107297

Contents lists available at ScienceDirect

Journal of Volcanology and Geothermal Research

journal homepage: www.elsevier.com/locate/jvolgeores

Hydrothermal alteration and sealing at Turrialba volcano, Costa Rica, as a mechanism for phreatic eruption triggering

Emily Mick [a,*], John Stix [a], J. Maarten de Moor [b], Geoffroy Avard [b]

[a] Department of Earth and Planetary Science, McGill University, 3450 University Street, Montreal, QC H3A 0E8, Canada
[b] Observatorio Volcanológico y Sismológico de Costa Rica (OVSICORI), Universidad Nacional, Campus Omar Dengo, Apartado Postal 2386-3000 Heredia, Costa Rica

ARTICLE INFO

Article history:
Received 4 December 2020
Received in revised form 17 May 2021
Accepted 21 May 2021
Available online 24 May 2021

Keywords:
Hydrothermal sealing
Turrialba volcano
Acid-sulphate alteration
Permeability

ABSTRACT

Turrialba is a basaltic to andesitic Holocene stratovolcano that after decades of quiescence re-activated in 1996 and has been highly active ever since. Turrialba is characterized by a highly active magmatic-hydrothermal system, and we propose that hydrothermal sealing and volatile accumulation are the mechanisms responsible for the reactivation and persistent phreatic activity at Turrialba since 2010. Evidence of sealing is found in pyroclastic breccias from phreatic eruptions as high concentrations of hydrothermal minerals coupled with low intrinsic permeability. The suite of volcanic breccias studied herein erupted from the main vent between 2014 and 2019 and has an alteration mineral assemblage of SiO_2 polymorphs ± gypsum ± natroalunite ± pyrite. The mineral assemblage is indicative of acid sulphate alteration within the advanced-argillic alteration facies characterized by temperatures of approximately 200–350 °C as indicated by the presence of gypsum and natroalunite, the high temperature endmember of the alunite series. Acid sulphate alteration is the result of extreme base leaching by acidic fluids (pH <4) with a high sulphate content. Measurements of permeability and porosity yielded variable porosity and very low to non-existent permeability in all hydrothermal breccia samples. Back-scatter electron (BSE) images reveal nano-, micro- and macro-scale fracture networks discontinuously filled with hydrothermal gypsum and pyrite which are responsible for diminished permeability, supporting the conclusion that hydrothermal sealing is active at Turrialba. Diminished permeability associated with the formation of a seal inhibits the escape of gases, causing them to accumulate below the seal and pressurize the system. Eventual seal failure due to overpressure results in the frequent phreatic eruptions seen at Turrialba.

1. Introduction

Phreatic eruptions are caused by the violent explosion of steam without the involvement of juvenile material resulting in lithic pyroclastic breccias and fall deposits (Barberi et al., 1992). Phreatic eruptions frequently have little to no warning, and the unpredictable nature of these eruptions places them among the most dangerous eruptions in crater areas. However, a lack of solid juvenile material does not imply that magma is not a factor in these eruptions; in many phreatic events magma plays an important role as the source of volatiles and heat that drive eruptions. This is the case when hydrothermal sealing is responsible for eruptions.

1.1. Phreatic eruptions and hydrothermal sealing

Hydrothermal sealing is a process by which fluids circulating in the magmatic-hydrothermal system below a volcano precipitate minerals within the vent area, reducing the permeability and essentially sealing the conduit by decreasing or stopping the escape of gases (Marinelli, 1969; Christenson et al., 2010; Stix and de Moor, 2018). Trapped below the seal, gases can accumulate until an overpressure threshold is reached and the seal fails, triggering a phreatic eruption (Marinelli, 1969; Stix and de Moor, 2018). Rocks forming the seal will therefore have low permeability and display signs of extensive hydrothermal alteration. The mineralogy of the seal will vary based on fluid chemistry and temperature and can include silica, clays and sulphur- bearing minerals (Stix and de Moor, 2018). The gases can be a mixture of hydrothermally-derived and magmatic gases. The depth of the seal and the depth of the hydrothermal system play important roles in the failure process. Shallow seals require less pressure to fail, and shallow hydrothermal systems cause less overpressure due to a comparatively small lithostatic overburden (Stix and de Moor, 2018). Explosive eruptions are frequently preceded by measurable increases in SO_2/CO_2, but the presence of a seal partially or fully preventing the escape of gases may have a significant impact on this important monitoring tool (de Moor et al., 2016b). A better understanding of this process is necessary to improve hazard management associated with such eruptions.

Since explosive eruptions resumed at Turrialba in 2010, phreatic and phreatomagmatic eruptions have been frequent. Hydrothermal sealing

* Corresponding author.
E-mail address: emily.mick@mail.mcgill.ca (E. Mick).

https://doi.org/10.1016/j.jvolgeores.2021.107297
0377-0273/

has been proposed as a mechanism for the persistent phreatic activity at Turrialba, but to date, no detailed study has been conducted to examine this concept (Stix and de Moor, 2018). Hence the goal of this study is to examine the subsurface processes responsible for phreatic eruptions at Turrialba, with general application elsewhere. For this study, a suite of pyroclastic breccia samples collected from the crater of Turrialba following phreatic eruptions in 2014, 2016, 2018 and 2019 were analyzed for their mineralogy and physical properties in order to examine the evidence of hydrothermal sealing. These breccias, sourced directly from the vent, can provide valuable insight into the physical process (i.e., reduction of permeability) of sealing in addition to the chemical processes (i.e., alteration) that may be discernible in other ejecta such as ash. In addition, we propose a conceptual model for the occurrence of sealing and phreatic eruptions at Turrialba and address the periodic nature of these events.

1.2. Turrialba volcano

Turrialba volcano, located roughly 60 km east of the capital San José, is the southernmost active volcano in Costa Rica and the second tallest stratovolcano at 3349 m a.s.l. (Fig. 1). Turrialba is characterized by basaltic to andesitic eruptive products, an active magmatic-hydrothermal system and abundant fumarolic activity (Vaselli et al., 2010; Campion et al., 2012). The volcano hosts three craters, east, west and central, that decrease in age from east to west with the western crater being the only currently active crater (Martini et al., 2010). Turrialba shares a common base with Irazú volcano, whose crater is located 10 km away; together, the two volcanoes form the largest volcano massif in Central America (Martini et al., 2010). Both Irazú and Turrialba are part of the Central American Volcanic Arc (CAVA), which is the result of the subduction of the Cocos plate beneath the Caribbean plate at a rate of approximately 70–85 mm per year (Fig. 1). The resulting arc extends from Costa Rica to the Mexico/Guatemala border (Whattam and Stern, 2016).

1.3. Eruptive history

In the 3500 years prior to the 20th century, Turrialba experienced six major eruptions in 1500 BCE, 1420 BCE, 800 BCE, 50C.E., 650C.E. and lastly in 1864–1866 (Soto, 1988; Alvarado, 2009). Following the 1864–1866 eruption, Turrialba entered a period of quiescence lasting until 1996, when reactivation was first detected; however, eruptive activity did not resume until 2010 (Reagan et al., 2006; Campion et al., 2012).

The 1864–1866 eruption of Turrialba began on August 17th, 1864, when ash fell throughout the Central Valley in Costa Rica including the capital of San José (Reagan et al., 2006). Phreatic explosions originated in the western crater and continued throughout most of the two-year period, producing ash columns that repeatedly distributed ash throughout the Central Valley. In the final two months of the eruption, January–February 1866, the eruptive character transitioned to phreatomagmatic. During this period of activity, juvenile basaltic clasts were ejected from the central crater. A final phreatic eruption from the western crater followed (Reagan et al., 2006).

Following the 1864–1866 eruption Turrialba entered a 130-year period of quiescence until 1996 when activity resumed, as evidenced by increasing seismicity and degassing. Important seismic swarms occurred in 2001, 2003, 2004, 2005 and 2007, each associated with increased gas flux and the opening of new fumarolic vents (Martini et al., 2010). Seismicity included a combination of long-period (LP) and volcano-tectonic (VT) events at depths of 4 to 6 km (Martini et al., 2010). Deformation during this time was measured with mixed results. Tilt measurements taken at various stations around the volcano detected inflation between 1996 and 2007; further inflation since 2010 has been detected using EDM and GNSS equipment (Martini et al., 2010; de Moor et al., 2016a).

Since reactivation in 1996 Turrialba has been carefully monitored, and three phases of activity have been identified based on both seismic activity and the activity of the magmatic-hydrothermal system as described by Vaselli et al. (2010) and Martini et al. (2010). The first phase, from 1996 to 2000, was characterized by low, constant seismicity accompanied by small fumarolic emissions from which magmatic components (e.g., SO_2) had been scrubbed by the hydrothermal system. The second phase, from 2001 to 2007, saw increased seismic activity and ground deformation as well as increased fumarolic activity and magmatic contributions. The final phase, which began in 2007, was marked by an important increase in fumarolic output and the transition to a composition dominated by magmatic fluids and ongoing seismic activity.

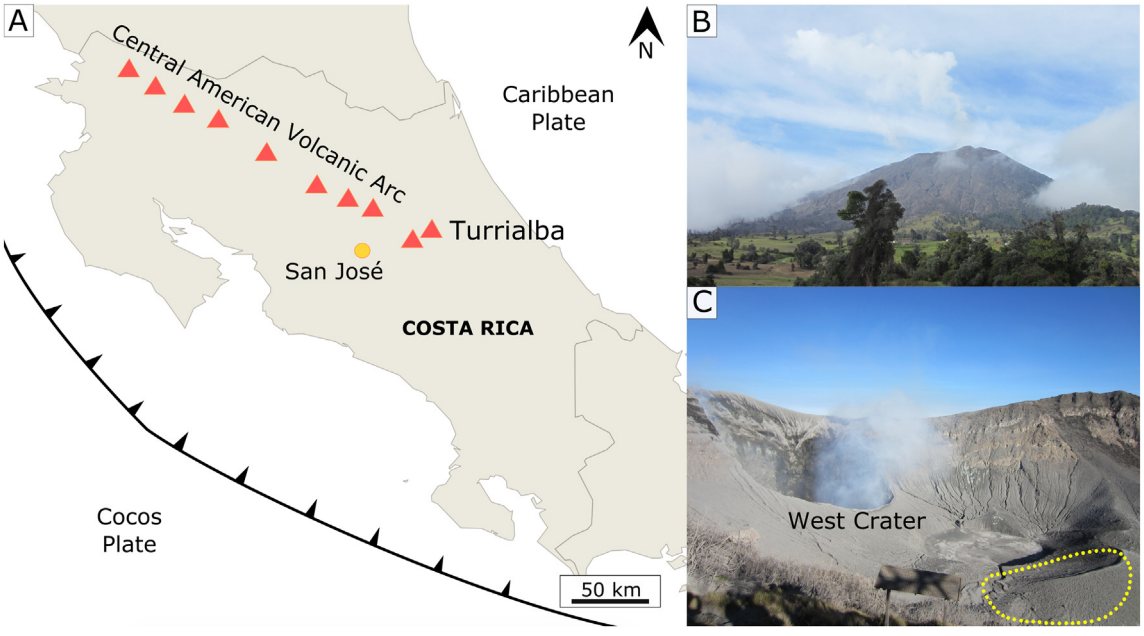

Fig. 1. A. Map of Costa Rica showing the location of Turrialba and other Costa Rican volcanoes of the Central American Volcanic Arc, as well as the Cocos-Caribbean subduction zone. B. View of Turrialba showing a faint gas plume among the clouds. C. View of the summit region of Turrialba showing the active west crater and the 2019 sampling area outlined in dotted yellow.

On January 5th, 2010, eruptive activity resumed at Turrialba with a phreatic eruption, opening a new fumarolic vent within the west crater (de Moor et al., 2016a). A second phreatic eruption took place on January 12th, 2012, again opening a new vent in the west crater, and on May 21st, 2013, both the 2010 and the 2012 vents experienced simultaneous gas eruptions (Global Volcanism Program, 2012; de Moor et al., 2016a). The next period of events, beginning on October 29th, 2014 and lasting until December 8th of the same year, included both phreatic and phreatomagmatic activity marking a new, more vigorous phase of activity at Turrialba (de Moor et al., 2016a; Alvarado et al., 2016; Global Volcanism Program, 2017). Since 2014 Turrialba has experienced nearly continuous degassing and frequent ash emissions. Phreatic eruptions have occurred repeatedly, associated with larger ash emissions, but have not been tracked separately (Global Volcanism Program, 2015; Global Volcanism Program, 2017; Global Volcanism Program, 2018; Global Volcanism Program, 2019a, 2019b). In 2017, fresh magmatic material was identified, up to 50% of eruptive products at the time, indicating that for a period the system was open to shallow magma below (de Moor et al., 2017).

2. Methods

2.1. Mineralogy

X-ray diffraction (XRD) analysis was performed on the ash matrix of all pyroclastic breccia samples in order to identify the composition and alteration of the ash. Matrix material was first isolated using a microdrill, taking care to avoid clasts, although clasts with a diameter less than 5 mm were difficult to avoid completely. The material was then sieved and the <400 μm fraction was placed in a tungsten carbide mill and ground for 90 s before being rinsed and placed back in the mill for a further 15 s of grinding. The sample was then dried on a watch glass in an oven at 30 °C, to avoid damaging possible clays, for up to three days until completely dry. The material was then sieved again and the <150 μm fraction used to prepare a back-packed slide. Analysis was performed using a Rigaku Smartlab X-Ray Diffractor with a copper target X-ray source and equipped with two detectors: a high-efficiency scintillation detector and a D/tex Ultra 250 high speed silicon strip 1D detector. Analyses were performed from 2 to 70 degrees using a step of 0.01 degrees and a speed of 1.0 s. The voltage was set to 40 kV and current to 44 mA. PDF-4 Minerals 2019 RBD software was used for data reduction, and PDXL2 Rigaku Data Analysis Software was used for confirmation, in order to ensure accuracy.

Further mineralogical analysis was performed using a scanning electron microscope (SEM) looking at both matrix and clast composition. Polished thin sections were prepared by Vancouver Petrographics Ltd. for a subset of 14 pyroclastic breccia samples. Preliminary mineral identification was done by transmitted light microscopy, and areas of interest were identified for detailed examination. The sections were then carbon coated, and SEM analysis was performed using a Hitachi SU5000 scanning electron microscope equipped with an energy dispersive X-ray spectrometer (EDS). Beam energy was set to 15 kV and beam current to 20 nA. Spot intensity was set to 50 when using EDS and 30 when imaging to minimize damage while the Z distance was set to 10 mm when using EDS and 5 mm when imaging. EDS analysis and processing were performed using Aztec version 3.3 software from Oxford Instruments.

2.2. Physical properties

Permeability and porosity were analyzed on a subset of 13 variably altered pyroclastic breccia and scoria samples. Seven breccia samples were omitted as they were of insufficient size for coring and analysis. Samples were first cored at INRS in Quebec City using a drill bit yielding 2.54 cm diameter cores through the thickest portion of the sample. The ends of each core were then cut and polished in order to form a perfect cylinder. Care was taken to limit any breakage along the edges which would alter the porosity values. All core lengths and diameters were then measured using a Mitutoyo electronic caliper, from which the volume was determined. Samples were then weighed, and density was determined. Porosity and permeability measurements were conducted using a Coretest Systems AP-603 combined permeameter-porosimeter. Porosity was first determined using grain volume measured using the Coretest Systems AP-603 and the previously determined total volume. Grain volume determinations occurred at atmospheric conditions as the chamber was unable to be pressurized. Multiple measurements of both porosity and permeability were then taken at 500 psi using nitrogen gas. Pressures of atmospheric and 500 psi were chosen to provide a range for the permeability of samples at low and high pressure. This is important since during sealing the pressure within the system would vary as gases accumulated. The associated software then performed a Klinkenberg correction to determine equivalent non-reactive liquid permeability values. Measurements at 500 psi failed when the permeability was below the detection limit; in these cases, the permeability was taken to be <0.001 mD, the detection limit of the instrument.

2.3. Fracture analysis

In order to quantify the fractures, EBS imaging was conducted using the SEM with the same settings as outlined above for imaging. The same 14 pyroclastic breccias used in the mineralogical study were analyzed. Fractures were imaged at scales of 500 μm, 400 μm, 300 μm, 200 μm and 100 μm. Fractures were then quantified in terms of connectivity using the method first described by Barton and Hsieh (1989). Connectivity was measured as the proportions of terminations, crossings, and abutments. To obtain a representative value, five fracture images at each scale were chosen, and the number of each type of fracture interaction was counted within each image. Images with the highest quality were selected for analysis in order to minimize error associated with visual identification of fractures. Care was also taken to include images from the maximum number of samples. During analysis fracture widths and wall types were also noted. Fractures were determined to fall within three scales: nano-, micro-, and macro-scale. The relative proportions of the three scales, as well as the distribution of filling by hydrothermal minerals, were then analyzed using the counting technique applied previously.

Fractures were then imaged in three dimensions within a representative breccia sample using a Xradia nano-CT instrument at the McGill Cell Imaging and Analysis Network. A preliminary, low-resolution scan was completed first to identify areas of interest, followed by a detailed, high-resolution scan of a smaller area. An initial scan with a pixel size of 40 μm was conducted followed by a secondary scan with a pixel size of 15 μm. Fractures were then mapped in 3-D using Dragonfly software by Open Research Systems.

Errors associated with fracture analysis may arise from several unavoidable sources. Firstly, it is impossible to discern which fractures have been formed as the result of the eruption of the breccias. This is noteworthy as fractures formed during the eruption would not have contributed to in situ permeability and therefore would not contribute to sealing or unsealing process prior to eruption. Secondly, given that pyroclastic breccias cannot be visualized at their source, i.e., within the vent, it is not possible to consider features beyond the scale of the bombs. Large, outcrop-scale fractures may have had an important effect on the overall permeability but cannot be evaluated following eruption as samples are no longer in situ.

3. Results

3.1. Mineral assemblage

All pyroclastic breccia samples show a high degree of alteration; very few samples contained any original mineralogy. However, some areas of

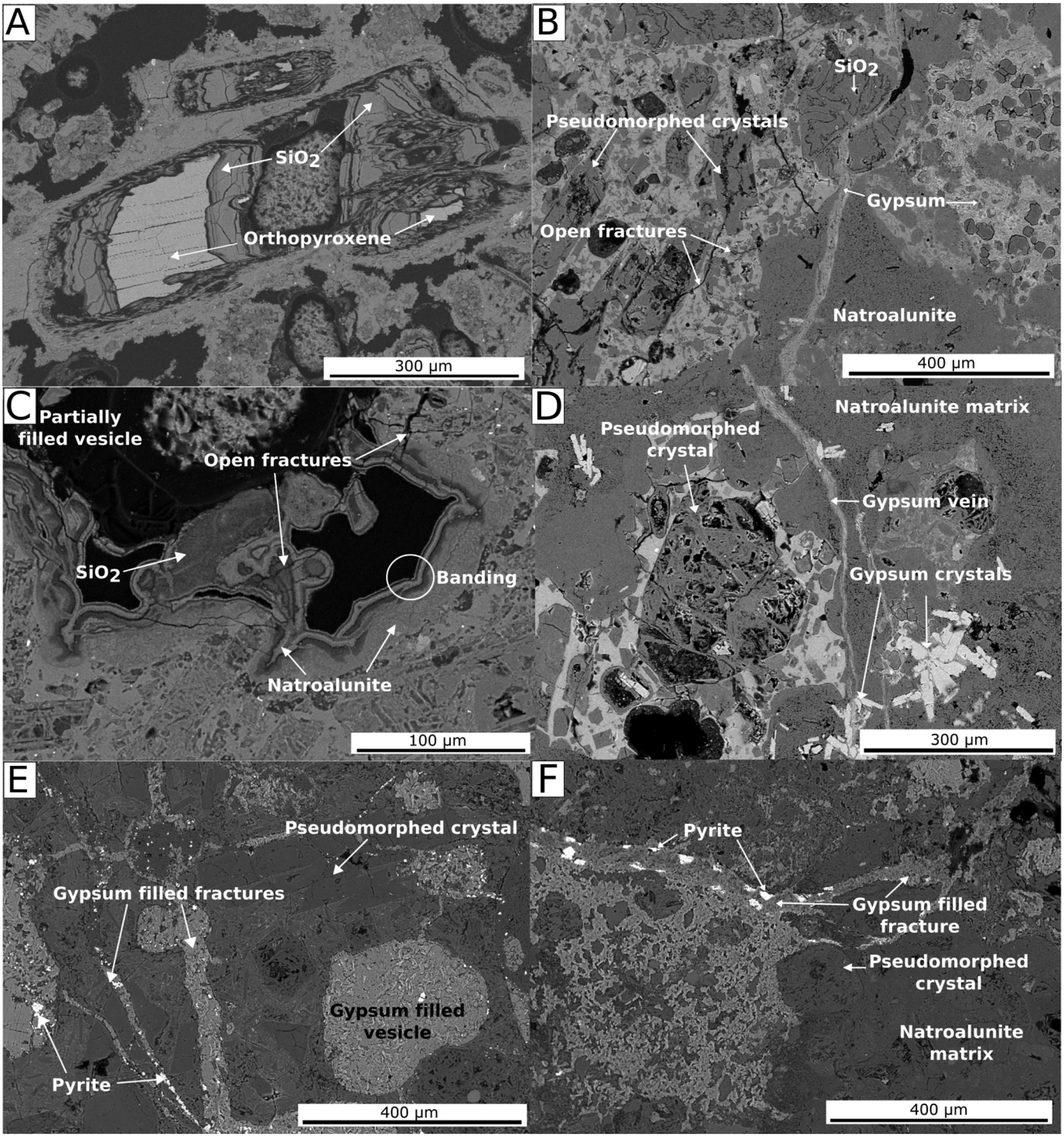

Fig. 2. Back-scattered electron (BSE) images. A: A large orthopyroxene crystal that has been partially altered to SiO_2. Sample T-18-11-07-R8. B: A thin gypsum-filled fracture cutting an area of fine-grained natroalunite. Thin open fractures cut small pseudomorphed crystals. Sample T-15-04-18-R1. C: A vesicle partially filled by several generations of SiO_2 and natroalunite seen as bands moving towards the center of the vesicle, all cut by younger open fractures. Sample T-18-11-07-R9. D: Continuous gypsum veins cutting a natroalunite matrix with discrete gypsum crystals. A pseudomorphed crystal of an unknown original composition now composed of mostly SiO_2 is also seen. Sample T-15-04-18-R1. E: Gypsum-filled fractures intersecting gypsum-filled vesicles in a vesicular basalt clast. Sample T-19-04-28-R8B. F: A thin vein of gypsum lined with pyrite that has been disseminated into the surrounding natroalunite matrix. Sample T-19-04-28-R8B.

primary igneous clinopyroxene, orthopyroxene and plagioclase are preserved in partially altered euhedral crystals (Fig. 2a). An alteration mineral assemblage of SiO_2 polymorphs ± gypsum ± natroalunite ± pyrite was identified both within the matrix using XRD and within the clasts using SEM (Table 1, Table 2). SiO_2 polymorphs including cristobalite and quartz were identified in all breccia samples as the primary component of pseudomorphed crystals as well as in the matrix as fine grained aggregates (Fig. 2b, c). Gypsum is the primary vein-forming and fracture/vesicle-filling mineral in the products of all major eruptions but is not present in every sample. Gypsum is manifested as

Table 1
Weight percent of matrix mineralogy of pyroclastic breccias determined by XRD. Data reduction was performed using PDF-4 Minerals 2019 RBD and PDXL2 Rigaku Data Analysis Software was used to confirm results. SiO_2 includes both quartz and cristobalite. Natroalunite includes natroalunite-1c, natroalunite-2c, and huangite. Only major minerals are included. All values are approximate and rounded to the nearest 5%. The term "present" denotes values <5%. Trace minerals including windhoekite, mawsonite, ankerite, ZnS and $Al_2(SO_4)_3$ were each identified on one occasion with wt% ≤5% but are omitted due to a lack of certainty associated with their low abundance and low occurrence. Full results including trace minerals and unrounded wt% available in supplementary data.

Sample number	Natroalunite	Alunite	Gypsum	Anhydrite	SiO_2	Albite	Anorthite	Pyrite
T-15-04-18 R1	95%		Present					
T-15-04-18 R2	95%		5%					
T-16-04-18 R1	95%		5%					
T-16-05-16 R2					Present		100%	
T-18-03-01 R1	30%		Present		10%	60%		
T-18-11-07 R8	90%				10%			
T-18-11-07 R9		100%						
T-18-11-07 R10			100%					
T-18-11-07 R11		65%	25%		5%			5%
T-19-04-28 R2							100%	
T-19-04-28 R3	80%		5%	10%	Present			5%
T-19-04-28 R4		85%			Present			15%
T-19-04-28 R5	15%		20%		Present	60%		
T-19-04-28 R6	85%		10%		5%			
T-19-04-28 R7	80%		5%		Present			15%
T-19-04-28 R8	75%		20%					5%
T-19-04-28 R9	100%		Present					
T-19-04-28 R10	80%		10%		10%			
T-19-04-28 R11	20%		10%		Present	70%		

fine-grained aggregates, distinct crystals and acicular needles both within the matrix and clasts (Fig. 2b, d, e). Natroalunite is present primarily as fine-grained aggregates in the matrix; it is rarely seen as radiating crystals within vesicles or accompanying SiO_2 in pseudomorphed crystals (Fig. 2c, f). Like gypsum, natroalunite is present in the products of all major eruptions but not all samples. Natroalunite is an aluminum sulphate mineral which, taken in combination with the dominant tabular form of the pseudomorphed crystals indicates that plagioclase was a major component of the original mineralogy. Pyrite is present as discrete grains, varying from cubic to amorphous, usually within veins or fractures filled by gypsum (Fig. 2e, f). Pyrite is observed only in samples from 2018 and 2019; no pyrite was identified in earlier samples and no other time-based variations were identified (Table 1, Table 2). Pyrite is the result of the interaction of H_2S-bearing fluids with Fe-bearing rocks or gypsum (Zimbelman et al., 2005). This is consistent with the association seen between pyrite and gypsum at Turrialba.

Based on cross-cutting relationships among veins, fractures and crystals, an alteration paragenesis has been developed. First a stage of leaching occurred in order to make available the elements seen in the replacement mineralogy. The banding of SiO_2 and natroalunite as seen in Fig. 2c, as well as the presence of both in some pseudomorphed crystals, indicates that SiO_2 and natroalunite replacement occurred simultaneously although SiO_2 was the dominant phase. Gypsum and pyrite appear to form a second phase of replacement as indicated primarily by gypsum veins cutting fully pseudomorphed crystals (Fig. 2b). At least two stages of fracturing occurred as well. Nearly all fractures are filled with gypsum rather than natroalunite or SiO_2, indicating that these fractures were likely formed after the initial stage of alteration. Many open and filled fractures also cut areas of SiO_2 and natroalunite alteration but are not filled by either, with only gypsum filling these fractures. The presence of large open fractures is suggestive of late-stage fracturing after the two stages of replacement, possibly caused by eruption of the breccia.

3.2. Physical properties

Permeability and porosity were measured for two fresh scoria samples (T-19-04-28-R1 and T-19-04-28-R12) and a subset of eleven pyroclastic breccias. A minimum core diameter and length of 2.54 cm was necessary for analysis, so some samples were not analyzed due to insufficient size. However, little variation was seen with regards to porosity and permeability of the tested samples, so we assume that the omitted samples have permeability and porosity values in the ranges below.

Table 2
Alteration assemblage and original mineralogy for pyroclastic breccia samples determined using SEM. SiO_2 includes both quartz and cristobalite.

Sample number	Alteration assemblage				Original mineralogy		
	SiO_2	Gypsum	Natroalunite	Pyrite	Clinopyroxene	Orthopyroxene	Plagioclase
T-15-04-18-R1	✓	✓	✓				
T-15-04-18-R2	✓	✓	✓		✓		
T-16-04-18-R1	✓	✓	✓				
T-16-05-16-R2	✓				✓		
T-18-03-01-R1	✓						
T-18-11-07-R8	✓					✓	
T-18-11-07-R9	✓	✓	✓	✓			
T-18-11-07-R10	✓	✓	✓		✓		
T-18-11-07-R11	✓	✓	✓				
T-19-04-28-R3	✓	✓	✓		✓	✓	
T-19-04-28-R4	✓			✓	✓	✓	
T-19-04-28-R5	✓	✓		✓	✓		✓
T-19-04-28-R7	✓	✓		✓	✓		✓
T-19-04-28-R8	✓	✓	✓	✓			

Table 3
Physical properties of selected hydrothermal breccias and fresh scoria samples (T-19-04-28-R1 and T-19-04-28-R12). Porosity at room temperature determined by grain volume. Porosity at 500 psi and gas permeability determined by a combined gas permeameter/porosimeter. Liquid permeability determined using a Klinkenberg correction.

Sample number	Density (Bulk)	Porosity (Room)	Porosity (500 psi)	Permeability (Gas)	Permeability (Liquid)
	kg/m^3	%	%	mD	mD
T-15-04-18-R1	1990	13.7	14.3	0.87	0.44
T-15-04-18-R2	2038	4.47	1.99	<0.001	<0.001
T-19-04-28-R1	1242	54.7	55.0	38.7	30.7
T-19-04-28-R2	1806	27.5	35.2	10.6	7.68
T-19-04-28-R3	1764	19.7	17.3	1.74	0.99
T-19-04-28-R5	1867	14.4	14.7	0.40	0.16
T-19-04-28-R6	1685	18.0	18.8	<0.001	<0.001
T-19-04-28-R7	1878	14.7	12.2	<0.001	<0.001
T-19-04-28-R8	2060	9.93	9.82	<0.001	<0.001
T-19-04-28-R9	1770	18.7	21.8	<0.001	<0.001
T-19-04-28-R10	2075	8.51	9.00	<0.001	<0.001
T-19-04-28-R11	2323	6.58	3.32	<0.001	<0.001
T-19-04-28-R12	1302	53.3	52.7	55.4	44.9

Porosity measurements at atmospheric conditions varied from 4.47% to 27.5% for pyroclastic breccias and from 53.3% to 54.7% for fresh scoria samples (Table 3). At 500 psi porosity varied from 1.99% to 35.2% for pyroclastic breccias, and from 52.7% to 55.0% for fresh scoria samples (Table 3, Fig. 3a). Porosity values are highly dependent on clast composition. At both atmospheric conditions and 500 psi, sample T-19-04-28-R2 was a clear outlier with significantly higher porosity than all other breccia samples (Fig. 3a). This sample is a clast-dominated breccia with exclusively vesicular basalt clasts. Samples with a higher percentage of vesicular clasts overall tended to have higher porosities. The porosity of any given sample varies no more than 3.26% between atmospheric conditions and 500 psi, again with the exception of sample T-19-04-28-R2 which has a difference of 7.72%. No porosity trends with respect to alteration were discernible.

Permeability values for gases varied from <0.001 mD to 10.6 mD for pyroclastic breccias and from 38.7 mD to 55.4 mD for fresh scoria samples (Table 3). Permeability values for liquids varied from <0.001 mD to 7.68 mD for pyroclastic breccias and from 30.7 mD to 44.9 mD for fresh scoria samples (Table 3, Fig. 3). As with porosity, sample T-19-04-28-R2 was an outlier with significantly higher permeability than all other breccia samples, 10.6 mD for gases and 7.68 mD for liquids. With the exception of this sample, all breccias had permeabilities below 1.74 mD for gasses and 0.99 mD for liquids.

Density values for pyroclastic breccia samples varied from 1685 kg/m^3 to 2323 kg/m^3 and from 1242 kg/m^3 to 1302 kg/m^3 for fresh scoria samples (Table 3, Fig. 3b). In all cases, the measured densities of the altered pyroclastic breccias fell below that of an average fresh andesite (2400 kg/m^3; Heap and Kennedy, 2016).

Given that pyroclastic breccias originate within a volcanic vent, they will generally undergo some degree of alteration. It is therefore difficult, if not impossible, to obtain an unaltered sample, and thus analogues are required. Fuller and Sharp (1992) conducted permeability measurements on fresh, altered and varnished samples of the Santana Tuff in Trans-Pecos Texas and obtained mean permeabilities of 55.33 mD, 5.03 mD and 3.31 mD respectively. This tuff varies in lithic composition and welding, hence it is not an exact analogue for an unaltered pyroclastic breccia. However, it does provide a range of permeability for explosive volcanic rocks. Heap et al. (2017) conducted permeability measurements on an assortment of minimally altered lava and variably altered lava breccia samples from White Island, New Zealand, another active andesitic stratovolcano. They found the lavas to have permeabilities of 1.80–11.25 mD, while lava breccias had permeabilities of 100.62–138.81 mD. Given the similarities between White Island and Turrialba, these lavas and lava breccias provide a reasonable proxy for the fresh equivalent of the pyroclastic breccias studied here. With this information, a significant loss of permeability through alteration is clear. As with porosity, however, no temporal trends with respect to alteration are discernible.

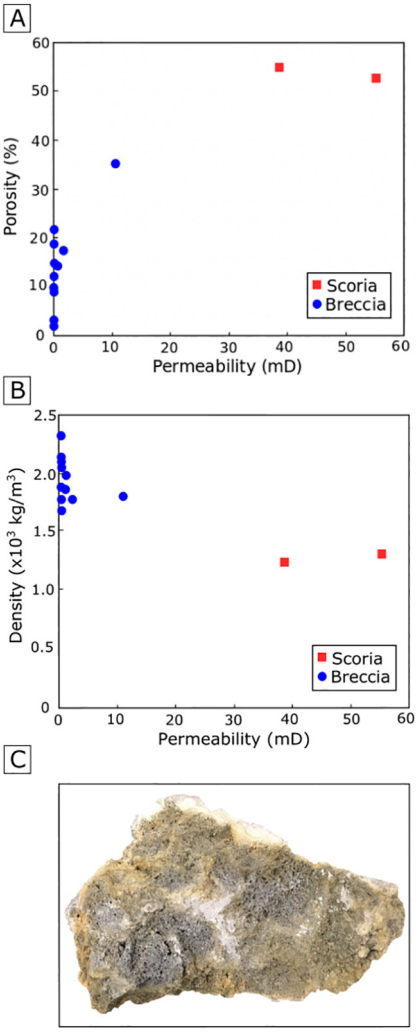

Fig. 3. A: Porosity (%) at 500 psi as a function of gas permeability (mD). B: Bulk density (kg/m^3) as a function of gas permeability (mD). C: Sample T-19-04-28-R2, a clast-dominated breccia with exclusively vesicular basalt clasts.

3.3. Fracturing

Fractures were analyzed qualitatively and quantitatively for multiple samples. Fracture connectivity was determined by looking at the proportions of the three types of fracture interactions: terminations, abutments and crossings. Results show that abutments, where one fracture ends as it intersects a second usually larger fracture, are the dominant feature within each scale of fracture analyzed (Fig. 4). Crossings, where two fractures intersect and both continue, as well as terminations, where a fracture ends, play less important roles. The dominance of abutments over other features is responsible for a general anastomosing character of the fracture networks seen at all scales (Fig. 5a, b). These observations indicate a high degree of connectivity.

Three primary scales of fractures are seen: macro-scale fractures with a width >10 μm, micro-fractures with a width of 1–10 μm and nano-scale fractures with a width <1 μm (Fig. 5b, c). Micro-scale fractures appear to be the dominant scale, with nano- and macro-fractures each responsible for a similar but lesser proportion of fractures

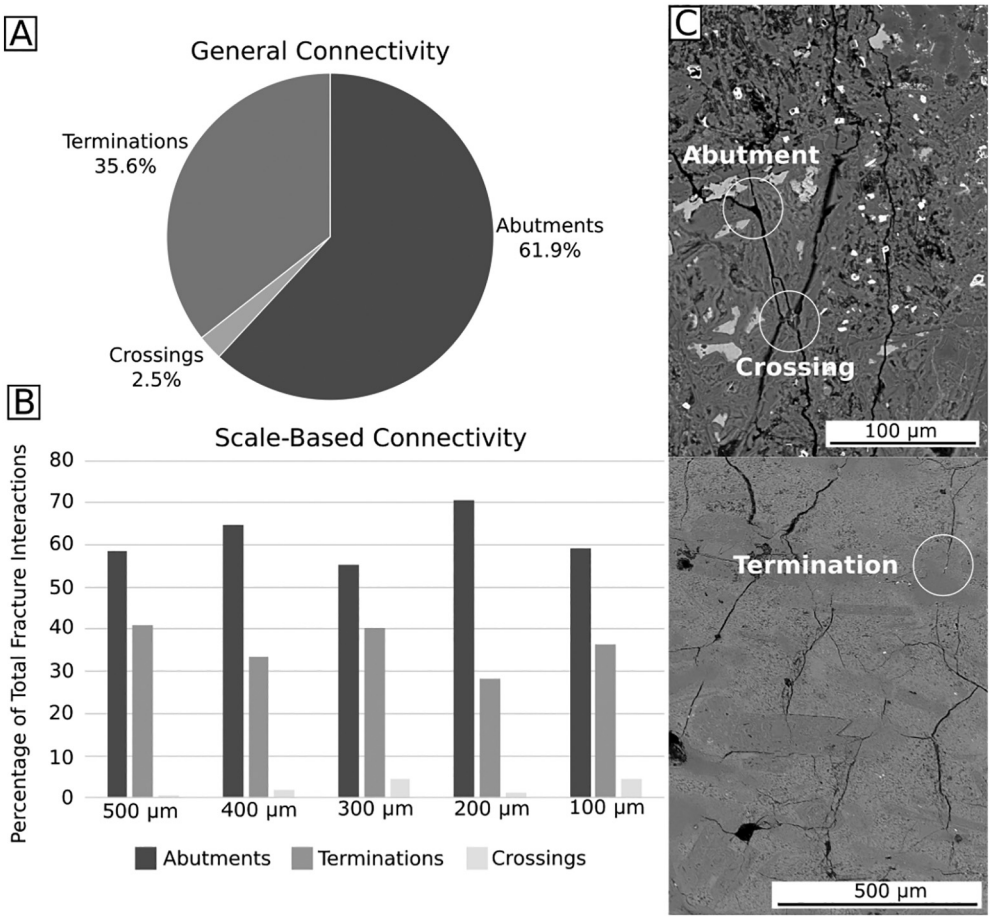

Fig. 4. Proportions of terminations, abutments, and crossings illustrate the degree of connectivity among pyroclastic breccia samples. A: General connectivity taking into consideration fractures at all scales. Intersections (abutments and crossings) are present in a higher proportion than terminations, indicating a high degree of connectivity. B: Connectivity features divided into five spatial scales. Intersections (abutments and crossings) are present in a higher proportion than terminations at all scales, demonstrating the general insensitivity of scale. C: Back-scattered electron (BSE) images showing examples of abutments, terminations and crossings.

(Fig. 6a). Macro- and micro-scale fractures are present in both matrix and clasts, but nano-scale fractures are only visible within clasts either in glass or crystals (Fig. 5c, d, e). Fractures are not restricted by the different media and can continue across clast and crystal boundaries (Fig. 5a). Instances of fractures surrounding clasts and crystals have also been noted, but this behavior is uncommon. Large fractures 1–5 mm in diameter are also visible at the sample scale although they are less common (Fig. 5f).

One aspect of fractures that does show variation between matrix and clasts is wall texture. Fractures within the matrix tend to display a rougher, more irregular wall texture, while fractures within clasts and crystals tend to have smooth walls (Fig. 5c, e). Fracture filling is also variable. As discussed above, fractures are filled with gypsum and occasionally pyrite; this is consistent across all samples. However, filling does not occur preferentially in any one media (i.e., matrix, clast or crystal), and open fractures are more prevalent than filled fractures at all scales (Fig. 6b). Filled and open fractures are present within all samples, and filling can be discontinuous within a single fracture (Fig. 7). It is worth noting that some fragile filling material may have been lost during seal rupture or sample processing; hence, proportions of open fractures are maximum values, and those of filled fractures are minimum values.

Connectivity is not a two-dimensional feature, so CT-scanning was used to image the fracture network in three-dimensions. The scans yield a series of images representing vertical slices through a rock core. In the four consecutive slices, each measuring 40 μm in thickness seen in Fig. 8, a group of fractures is shown to connect over 160 μm in thickness. In each image, fractures appear to show several terminations, but in sequence it is clear that an individual fracture continues in the vertical dimension and the terminations may in fact represent a change in fracture orientation. The high degree of three-dimensional connectivity leads us to believe that a significant portion of apparent fracture terminations noted in two dimensions are in fact continuous in the third dimension. The fact that they appear to terminate is the result of a lack of visualization in the third dimension. Hence our connectivity values (Fig. 4) are minimums.

4. Discussion

Analysis of hydrothermally altered breccias in terms of mineralogy and physical properties has provided new information regarding the mechanism responsible for phreatic eruptions at Turrialba. In the following sections we discuss this evidence and the possible mechanisms for these eruptions and hydrothermal sealing at Turrialba and elsewhere.

4.1. Examples of hydrothermal sealing and phreatic eruptions: Ruapehu and Ontake

Hydrothermal sealing has been studied as the cause of several well-known phreatic or phreatomagmatic eruptions. Here we examine eruptions at two volcanoes, Ruapehu in 2007 and Ontake in 2014. Ruapehu, on the North Island of New Zealand, is an andesitic stratovolcano that has undergone frequent phreatic and phreatomagmatic eruptions throughout the second half of the 20th century (Christenson and Wood, 1993). In 2007 Ruapehu experienced a small phreatomagmatic

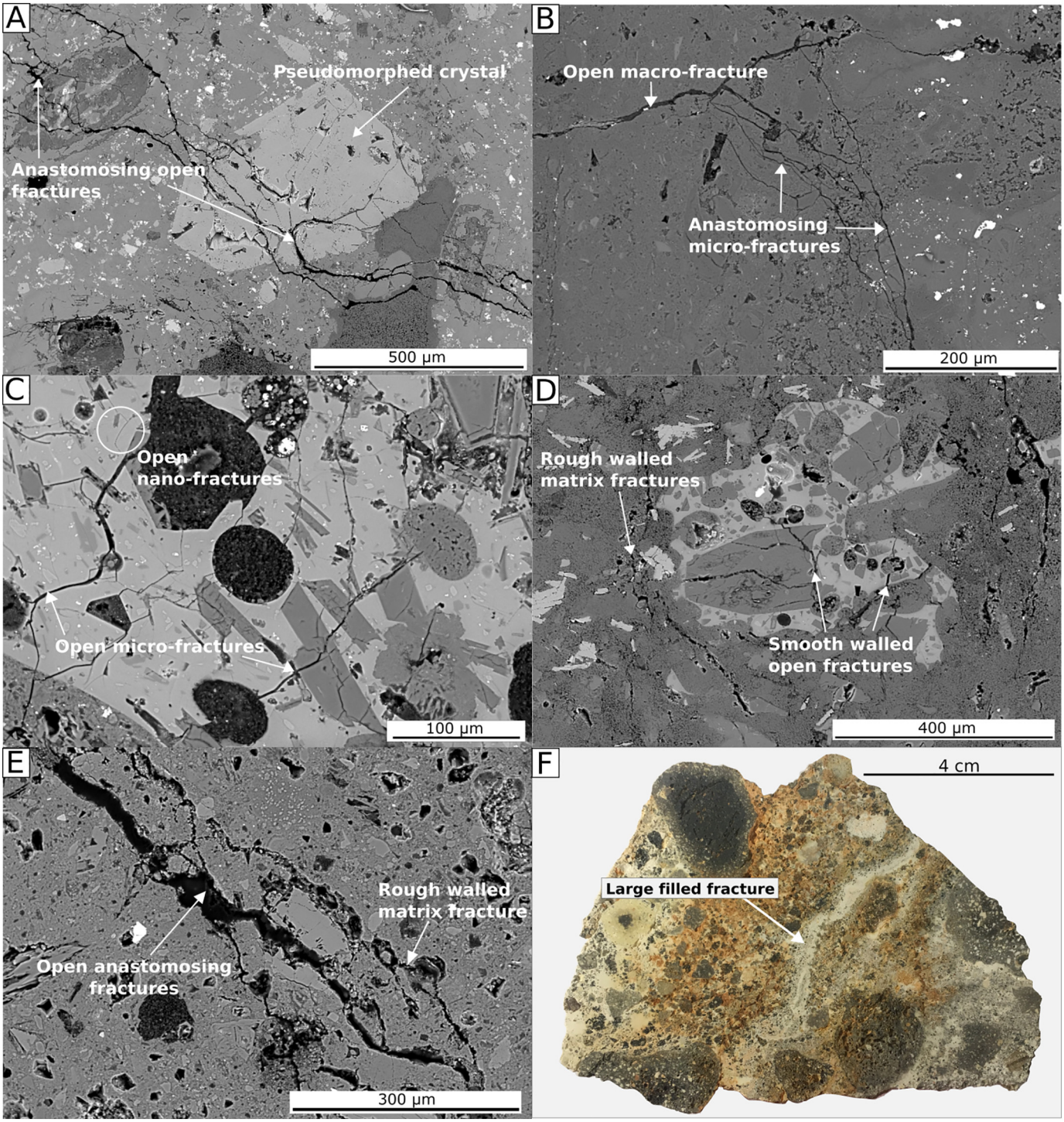

Fig. 5. Back-scattered electron (BSE) images. A: Continuous open and anastomosing fractures transecting a pseudomorphed crystal. B: Open macro-fractures and anastomosing micro-fractures. C: Open continuous micro-fractures and nano-fractures within a basalt clast. D: Smooth walled fractures within a basalt clast surrounded by matrix containing rough walled fractures. E: Open, anastomosing, irregular macro-fractures within the matrix. F: Large filled fracture within a pyroclastic breccia sample.

eruption without warning, resulting in ejecta traveling as far as 2.5 km from the crater (Christenson et al., 2010). Ruapehu hosts a crater lake known to undergo thermal cycling between 10 °C and 60 °C over periods of 4 to 16 months (Christenson et al., 2010). Eruptions at Ruapehu tend to occur during periods of high heat flow and elevated lake temperatures. At the time of the eruption on September 25th, 2007, however, the lake temperature was only 13 °C (Christenson and Wood, 1993; Kilgour et al., 2010). The event consisted of a block and ash eruption accompanied by a surtseyan jet and several lahars, aided by the fact that the crater lake was already at overflow levels (Kilgour et al., 2010). In the 10 min prior to the onset of eruptive activity, a small volcano-tectonic earthquake (VT), a very long period (VLP) event and a burst of tremors were recorded, but this was insufficient warning to enact adequate protection measures (Mordret et al., 2010; Christenson et al., 2010). Within the erupted material, highly altered blocks with low permeability were found, indicating that hydrothermal

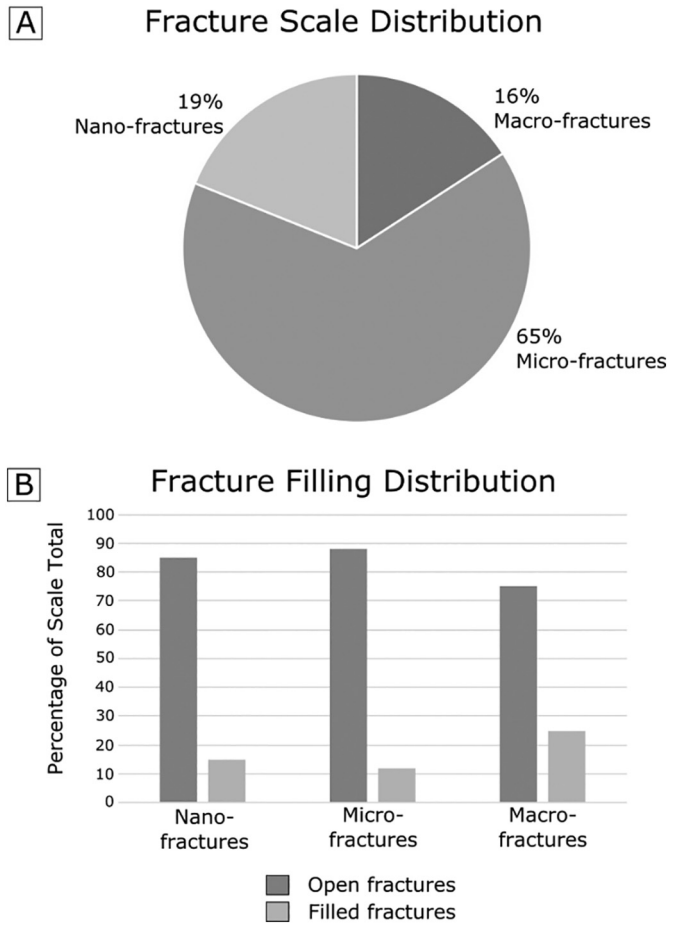

Fig. 6. A: Distribution of macro-scale fractures with a width > 10 μm, micro-fractures with a width of 1–10 μm and nano-scale fractures with a width <1 μm. B: Distribution of filled and open fractures within each fracture scale.

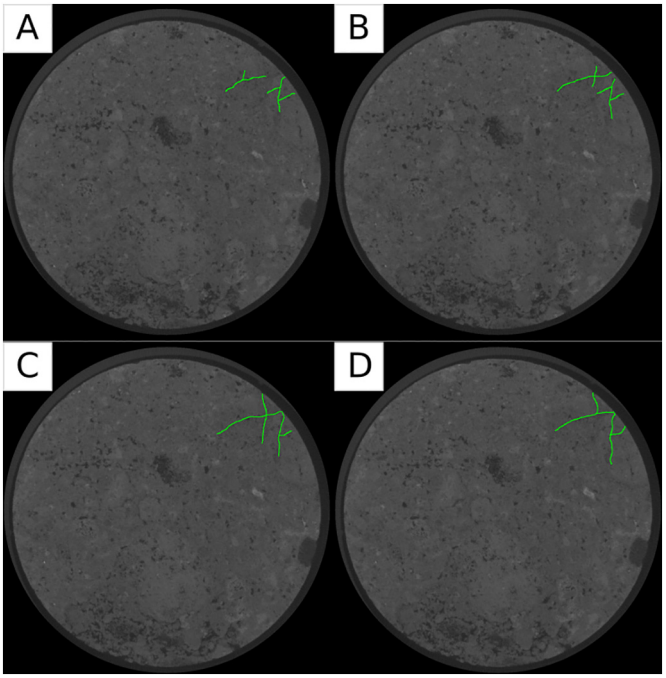

Fig. 8. Four consecutive vertical core slices obtained by CT-imaging showing the 3-dimensional connectivity of fractures. Each image is separated by a thickness of 40 μm.

sealing was at least partly responsible for this eruption (Christenson et al., 2010). Additionally, despite being actively removed from the system via scrubbing, low SO_2 flux values show a slight increasing trend coupled with decreasing CO_2 in the year prior to the eruption suggestive of the formation of a sulphur seal at a shallow level. An increase in gas emissions and CO_2 enrichment of the gases for the three days following the eruption also support the presence of a seal which had been ruptured (Christenson et al., 2010). Following the initial period of high CO_2 after the eruption, a change towards high SO_2/CO_2 indicated that the system had transitioned into a magmatic stage of activity (Christenson et al., 2010).

Recent activity at Mount Ontake in central Japan began in 1979, and since then three eruptions have occurred in 1991, 2007 and 2014 (Kaneko et al., 2016). On September 27th, 2014 Ontake erupted suddenly with little to no warning, resulting in the deaths of 60 people hiking in the area (Kaneko et al., 2016). The 2014 eruption was characterized by a plume reaching 7.8 km above the crater and eruptive material composed primarily of altered non-juvenile material with a small juvenile component (Oikawa et al., 2016; Miyagi et al., 2020). Hence the eruption was phreatomagmatic rather than phreatic. Hydrothermal minerals including sulphates (gypsum, alunite, anhydrite), clays (kaolin minerals) and cristobalite were all present in the ejecta (Ikehata and Maruoka, 2016). As is common with phreatic eruptions caused by sealing, very little warning preceded this eruption. Workers located in huts on the mountain noted that no rumbling, ground motion

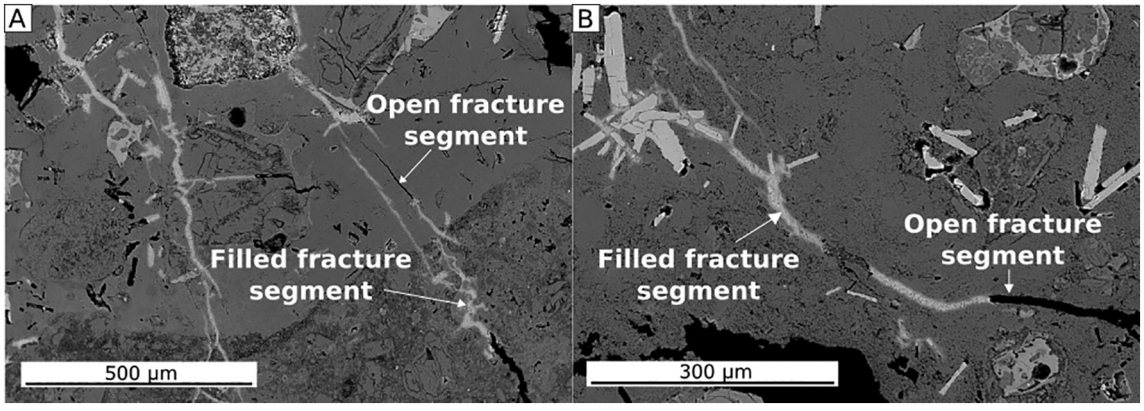

Fig. 7. Back-scattered electron (BSE) images. In each image, fractures show both open and filled segments. A: Discontinuous filling of a fracture cutting through matrix and clast material. B: Discontinuous filling of a matrix fracture.

or sulphur smell were present prior to the eruption (Oikawa et al., 2016). However, an increase in seismicity was noted in early September 2014 but subsided after September 16th (Kato et al., 2015). Increased seismicity was not observed again until volcanic tremors began 11 min prior to the eruption, followed by a rapid inflation of the edifice and laterally migrating VT earthquakes (Kato et al., 2015; Kaneko et al., 2016). The migrating VT earthquakes and inflation are believed to result from rapid movement of pressurized fluids through the conduit, which taken together with the ejecta composition indicate that hydrothermal sealing was a factor in this eruption (Kato et al., 2015). The actual seal rupture is believed to be responsible for the first, less explosive gas phase of the eruption, while the sudden decompression that followed caused rapid boiling of water and a second more explosive phase of activity responsible for most ejecta (Kaneko et al., 2016). Following the eruption, a sustained SO_2 flux of >100 t/day in addition to elevated SO_2/H_2S was taken to indicate a sustained magmatic fluid supply into the hydrothermal system (Mori et al., 2016).

These two examples show several important similarities. (1) Little to no warning occurred prior to either eruption. The unpredictable nature of phreatic and phreatomagmatic events, in particular those related to hydrothermal sealing, is responsible for the fact that these eruptions are among the most dangerous, Ruapehu and Ontake included. While both volcanoes did exhibit some seismic warning signals, they were limited to several minutes prior to the eruptions, and other common warning signals were absent. At Ruapehu the eruption was unexpected given the low lake temperatures contrary to previous eruptions. (2) Ejecta from both eruptions display a high degree of alteration dominated by hydrothermal minerals including sulphates, clays and silica resulting in low permeability of the ejecta. (3) Eruptive products from both systems were dominantly lithic and altered, while a small juvenile component was also recognized. Hence both eruptions were phreatomagmatic, not phreatic. (4) Following the eruption at Ruapehu, changes in the gas composition and rate of degassing were typical of a seal that had broken, namely an increase in SO_2 and CO_2 gas emissions and magmatic SO_2/CO_2 signatures of the gases. Similarly, SO_2 fluxes and SO_2/H_2S ratios at Ontake reflected magmatic fluid contributions after eruption. For both systems, the eruptions appear to have opened the plumbing system for a period of time, allowing magmatic gases to move through and exit the volcano.

4.2. Hydrothermal alteration at Turrialba

The alteration mineral assemblage at Turrialba consists of SiO_2 polymorphs ± gypsum ± natroalunite ± pyrite indicative of acid sulphate alteration (Table 1, Table 2; Armstrong, 1995; Zimbelman et al., 2005). Acid sulphate alteration is common at volcanoes worldwide and is characterized by acidic fluids resulting in extreme leaching followed by precipitation of primarily sulphate and sulphide minerals (Armstrong, 1995; Heap et al., 2019). A source of sulphur is an essential component of acid sulphate alteration. In andesitic stratovolcanoes such as Turrialba, isotopic data indicate that sulphate and sulphide alteration minerals are the result of the disproportionation of magmatic SO_2 to form the aqueous sulphate required for alteration (Meyer and Hemley, 1967; Zimbelman et al., 2005). The near-surface oxidation of H_2S may provide a secondary source of sulphate (Stoffregen, 1987).

The alteration mineralogy is indicative of a pre-alteration mineral assemblage consisting of feldspar and pyroxene (Minami et al., 2016). Alunite is typically the product of alkali feldspar leaching, but the dominance of natroalunite containing Ca and Na rather than K indicates that plagioclase is the dominant feldspar phase at Turrialba (Armstrong, 1995). The preserved primary igneous minerals include plagioclase, orthopyroxene and clinopyroxene (Reagan et al., 2006; Table 2).

Acid-sulphate alteration also falls within the field of advanced argillic alteration which is characterized by extreme leaching of cations other than Al and Si followed by sulphate and sulphide deposition, including but not limited to alunite group minerals, secondary silica, gypsum and pyrite (Meyer and Hemley, 1967; Stoffregen, 1987; Henley and Berger, 2011; Minami et al., 2016). The assemblage seen at Turrialba is typical of this type of alteration, with the exception of the lack of clay minerals, kaolinite being the most common in such settings. During advanced argillic alteration, alunite group minerals can substitute for clays; given the proper ion availability from feldspars, alunite and natroalunite can form from the reaction of kaolinite with aqueous sulphate, H^+ and K^+ (Stoffregen et al., 2000; Henley and Berger, 2011). Plagioclase is an important component of the primary igneous mineralogy, although it has now been largely replaced by SiO_2. Furthermore, SO_2 is known to be abundant at Turrialba providing the necessary components for the formation of natroalunite in place of clay minerals (Vaselli et al., 2010). Kaolinite is not present in any of our samples indicating that temperatures are likely higher than 200 °C at which point kaolinite is no longer stable (John et al., 2008). Alteration in systems such as Turrialba occurs in zones (e.g., Minami et al., 2016), with advanced argillic/acid-sulphate alteration occupying most of the central area. It is possible that the alteration has produced clays such as kaolinite in areas further from the vent where sulphate is less abundant and temperatures are cooler. However, the breccias analyzed here are sourced directly from the vent area and have therefore exposed to the most SO_2 enriched gases and the highest temperatures (John et al., 2008).

The alteration mineral assemblage is consistent for all samples. With the exception of pyrite which as noted above is only present in later samples, no time-based variations in mineralogy are seen. Given that pyrite is not present in all later samples but rather in only a select few, this is likely due to sampling bias rather than a change in chemistry, as more samples were collected following later eruptions (Table 1, Table 2). In addition, pyrite is the least abundant major mineral and therefore could be missing in some samples. The consistent alteration indicates that the magmatic-hydrothermal system at Turrialba has not undergone any major changes between 2014 and 2019 and is likely still in the third phase of activity since reactivation, as described by Vaselli et al. (2010) and Martini et al. (2010), with a dominance of magmatic contributions over hydrothermal contributions.

Given the alteration mineralogy, it is possible to make estimates with respect to the fluids responsible for the alteration. Acid-sulphate alteration is the product of extreme leaching by acidic fluids. The pH of these fluids can vary but is typically less than 4 as indicated by the presence of natroalunite (Rodriguez and van Bergen, 2017). Most minerals within the assemblage are stable across a very wide range of temperatures, hence the temperature of alteration is difficult to constrain. Alunite group minerals including natroalunite are typically associated with temperatures of 200–350 °C but are stable to temperatures upwards of 380–450 °C (Meyer and Hemley, 1967; Henley and Berger, 2011; Heap et al., 2019). Gypsum and its hemihydrated form bassenite are stable at temperatures of <50 °C to upwards of 200 °C at high pressure (Klimchouk, 1996). Based on the alteration, we propose that the fluids at Turrialba have pH <4 and temperatures between 200 and 350 °C. As noted in the mineral paragenesis, it appears that alteration has occurred in two separate stages. A first stage consisting of the deposition of SiO_2 and natroalunite was followed by the deposition of gypsum in a later stage of alteration. We believe this is the result of the differing temperature requirements of the minerals. Natroalunite and SiO_2 would have been deposited first at high temperature, beginning the sealing process and allowing pressure to build. A second, lower-temperature stage then allowed for the deposition of gypsum, causing further sealing. Similar alteration at Merapi volcano was found to be the result of fluids with a pH <3 and temperatures ;/;200 °C (Heap et al., 2019). Conditions corresponding with advanced argillic and therefore acid-sulphate alteration are believed to occur between the surface and 2 km depth (Minami et al., 2016). It is known that Turrialba hosts a shallow hydrothermal system and a magma reservoir as shallow as 1 km below the surface (Di Piazza et al., 2015; Rizzo et al., 2016). Hence, we propose that this alteration occurred within the uppermost kilometer of the system.

A potential additional stage of alteration exists in the form of post-eruptive alteration. All samples analyzed herein were collected from the crater of Turrialba in the weeks to months following their eruption. Given the high level of activity at Turrialba, these samples will in all likelihood have been exposed to high levels of volcanic gases. Some samples feature surficial fine-grained native sulphur, but this alteration is limited to the exposed surface of the sample. Exposure at the surface may also have resulted in the dehydration of anhydrite to gypsum; however, no replacement textures were noted with respect to the gypsum replacing anhydrite.

4.3. Permeability and fracturing

Permeability and porosity are important factors in hydrothermal sealing as they control the movement of fluids and gases through a rock. Hydrothermal alteration can both increase and decrease permeability and porosity through mineral breakdown and mineral replacement respectively (Mordensky et al., 2019). We determined above that lava and lava breccia samples from White Island, New Zealand, analyzed by Heap et al. (2017) could be used as an analogue for unaltered pyroclastic breccia samples. They found the lavas to have permeabilities of 1.80–11.25 mD, while lava breccias had permeabilities of 100.62–138.81 mD. With the exception of sample T-19-04-28-R2, a vesicular basalt clast-dominated breccia, no permeability values of pyroclastic breccias at Turrialba exceed the lowest fresh estimate of 1.80 mD. This indicates that precipitation has dominated over dissolution, and hydrothermal alteration of the breccia samples has caused a reduction in permeability. Previous studies have found that hydrothermal alteration can lower the permeability of samples by up to four orders of magnitude which is consistent with our findings (Heap et al., 2017; Heap et al., 2019; Farquharson et al., 2019). The processes of dissolution and precipitation are both likely to be occurring within the system, but the balance between them may vary. Given the high degree of replacement seen within most mineral grains (Fig. 2a, b, d), we propose that a period dominated by dissolution likely preceded the precipitation that resulted in a loss of permeability.

Some samples display very low permeability values but relatively high porosity values. For example, sample T-19-04-28-R9 has a permeability of <0.001 mD but porosity values of 18.7–21.8% (Table 3). Discrepancies between permeability and porosity values are likely due to fractures being responsible for only a certain portion of the overall porosity, meaning a large decrease in permeability due to fracture filling would have a relatively small effect on porosity (Heap et al., 2019; Farquharson et al., 2019).

Permeability, however, is not simply a factor of porosity; it is influenced by fracture connectivity (Heap et al., 2017). As shown in Fig. 5, the breccia samples host complex networks of nano-, micro- and macro-scale fractures that are variably filled with hydrothermal minerals. Well-connected fracture networks as seen here are typical of moderate to high porosity volcanic rocks (Heap and Kennedy, 2016). Our analysis demonstrates that breccias from Turrialba display a high degree of connectivity among both filled and open fractures (Fig. 4). This connectivity is supported by the lack of variation for permeability and porosity values (Table 3, Fig. 3). The high degree of connectivity among fractures is indicative of moderate permeability, yet our measured values indicate that the breccia samples have a very low permeability, supporting the conclusion that hydrothermal alteration has resulted in an important loss of permeability. This poses a paradox since a majority of fractures at all scales are open rather than filled (Fig. 6b). As shown previously, however, filling is frequently observed to be discontinuous (Fig. 7). As a result of this discontinuous hydrothermal filling, a significant portion of fractures that appear "open" are in fact blocked by filling elsewhere in the fracture network and therefore do not contribute to the overall permeability. Additionally, a portion of fractures were likely the result of the eruption process and therefore will not have been subjected to fracture filling.

Fracturing does not appear to occur preferentially in one media, but the media type does nonetheless affect the nature of the fracturing and therefore permeability. For example, fractures within the matrix display a rough, irregular wall texture in comparison to fractures within clasts and crystals (Fig. 5c, d, e). This is due to the granular nature of the matrix as compared to the fine-grained glassy nature of the clasts. Fractures with rough walls can disrupt fluid flow, thus tend towards lower permeability (Heap and Kennedy, 2016). Therefore, the abundance of matrix within a sample and the distribution of fractures between the matrix and clasts will impact permeability. Additionally, nano-scale fractures were only found within crystals and clasts (Fig. 5c). This is again believed to be due to the fine-grained glassy nature of the media, but as these fractures tend to be discontinuous, their effect on permeability would be limited. However, their presence does affect the overall connectivity.

As noted above, fracturing appears to have occurred in several stages rather than as a singular event. It is not possible to discern the precise number of stages, but several causes have likely played a role. Firstly, as discussed above, a portion of the fractures are likely the result of the phreatic eruptions that produced the breccia samples. The pressure and energy associated with seal rupturing and the ensuing phreatic eruptions result in large-scale fractures that open the vent and can also form the small-scale fractures seen within all samples. Secondly fracturing may be the result of seismic activity. Many seismic swarms have been associated with the reactivation of Turrialba, in addition to ongoing seismic activity common to active volcanoes. Lastly, fractures may be due to an accumulation of pressure either within the hydrothermal system or from an accumulation of magmatic gases. All these sources of fractures are recurring within the system and can thus be responsible for multiple generations of filled and open fractures.

4.4. Hydrothermal sealing at Turrialba

Hydrothermal sealing occurs when fluids within the magmatic-hydrothermal system of an active volcano deposit hydrothermal minerals including SiO_2 polymorphs, sulphate species and clays within the shallow subsurface of the volcano (upper 1–2 km) including the vent, thus reducing the permeability of the vent material and allowing for gas and pressure buildup. The rocks forming this seal will display a high degree of alteration, host significant hydrothermal mineralization, and display low intrinsic permeability (Christenson et al., 2010). As demonstrated above, the pyroclastic breccia samples collected at Turrialba produced by eruptions in 2014–2019 have been heavily altered by acid-sulphate fluids resulting in an abundance of hydrothermal minerals including SiO_2 polymorphs $\pm$ gypsum $\pm$ natroalunite $\pm$ pyrite. Using an analogue for a fresh equivalent, we can also determine that this alteration has resulted in a significant decrease in permeability due to the filling of the complex fracture networks present. Previous work by Heap et al. (2017) found that acid sulphate fluids reduce the permeability of shallow volcanic rocks due to the deposition of alunite-group minerals, supporting our finding that the reduction in permeability at Turrialba is due to alteration and not another mechanism. We therefore conclude that these pyroclastic breccia samples are samples of multiple failed hydrothermal seals formed at Turrialba since 2014 which are responsible for the frequent phreatic eruptions seen.

Seals may fail due to either chemical or mechanical breakdown. Chemical breakdown of a seal as a result of changes within the magmatic-hydrothermal system will likely allow for the gradual venting of pressure and thus is unlikely to trigger an eruption. Mechanical breakdown of a hydrothermal seal is the result of an accumulation of pressure below the seal until a certain overpressure is reached, resulting in the failure of the rocks forming the seal and the sudden release of pressure. The mechanical breakdown of seals is believed to trigger phreatic eruptions.

Previous studies of volcanic gases at Turrialba provide additional evidence for hydrothermal sealing. In the weeks prior to the October 29th, 2014 eruption, de Moor et al. (2016a) noted that both SO_2 and CO_2 flux values were very low at Turrialba, indicating the possibility of a seal inhibiting the escape of gas. Following the December 9th, 2014 eruption, the same study noted a dramatic increase in gas fluxes immediately following the eruption. Along with erratic pre-eruptive gas fluxes, a sudden increase in gas flux after a phreatic eruption is strong evidence for the rupture of the hydrothermal seal (Christenson and Tassi, 2015). Such post-eruptive increases have been observed at Ruapehu, Ontake, and Turrialba.

Hydrothermal sealing occurs by degrees, and a complete seal is not necessary in order for phreatic eruptions to be triggered. More complete seals are likely to accumulate gas more quickly at a constant input, but it is only necessary for the flow of gas into the system from below to exceed the rate of gas escape in order for pressure to accumulate. A near continuous plume of gas present at Turrialba since 2014 may indicate that sealing is only partial (de Moor et al., 2016a). Another important consideration is the strength of the rock forming the seal. A stronger rock will be able to withstand higher pressures before cracking. Therefore, a seal formed within stronger rocks will likely require higher pressures for the seal to fail. This is likely to lead to less frequent but larger eruptions.

The timescale at which sealing is active is also an important feature to consider. The frequent phreatic eruptions at Turrialba since 2010 indicate that sealing is a recurring process and occurs on a relatively short timescale, on the order of months to a year or more. In addition, as this is based on the frequency of seal failure, it is possible that seals are forming on an even shorter timescale, as the rate of gas accumulation as well as the rate of sealing and the strength of the seal will all affect the frequency of seal failure. We propose that sealing could occur on timescales as short as days to weeks when small amounts of hydrothermal minerals cause a rapid reduction in permeability of the system. This is suggested by (1) the discontinuous fracture filling (Fig. 7) and (2) the irregular, anastomosing network of micro-fractures wherein a small area of filling may effectively seal a much larger portion of the fracture network (Fig. 5a, b). Such permeability decreases could quickly drive the system across a sealing threshold, generating the overpressure necessary for seal rupture and eruption. Finally, it is likely that sealing will continue as long as the magmatic-hydrothermal system remains in its current state as described by Vaselli et al. (2010) and Martini et al. (2010).

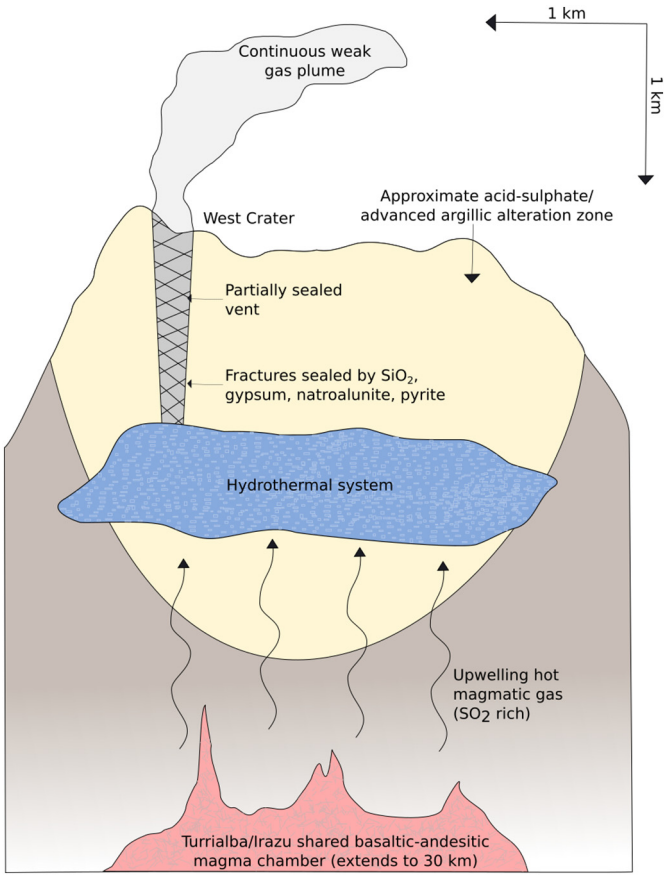

Fig. 9. Diagram of hydrothermal sealing at Turrialba adapted from Stix and de Moor (2018). Magmatic gases originating in the magma reservoir extending from between 1 and 10 km below the surface up to depths of 30 km (Di Piazza et al., 2015) enter the shallow hydrothermal system (Rizzo et al., 2016). Newly formed hot (200–350 °C), acidic (pH <4) fluids cause the dissolution of primary igneous minerals and the precipitation of hydrothermal minerals within the permeable conduit, sealing fractures.

4.5. Hydrothermal sealing model

Sealing at Turrialba occurs when hot magmatic gases released from the shallow magmatic system (1–10 km from the surface; Di Piazza et al., 2015) below the crater travel upwards, entering and dissolving in the hydrothermal system (Fig. 9). The introduction of these magmatic gases results in the formation of acid-sulphate fluids with a pH <4 and temperatures ranging from 200 to 350 °C (Meyer and Hemley, 1967; Klimchouk, 1996; Henley and Berger, 2011; Rodriguez and van Bergen, 2017; Heap et al., 2019). The acidic fluids cause the leaching and subsequent deposition of the alteration mineral assemblage (SiO_2 polymorphs ± gypsum ± natroalunite ± pyrite) within the vent (upper 1–2 km of the volcano) in a two-stage depositional process. The deposition of alteration minerals within the fracture network causes the gradual restriction of flow within some fractures while fully closing other fractures. These fractures formed prior to sealing as outlined above. The restriction of fractures at key points within the fracture network would result in a reduction in permeability within the vent thus forming a hydrothermal seal. In all likelihood Turrialba hosts only a partial seal. The seal nevertheless allows for the accumulation of hydrothermal and magmatic gases within the vent allowing for an accumulation of pressure until sufficient overpressure is reached. Overpressure will result in the mechanical failure of the seal and the formation of additional fractures, ultimately resulting in a phreatic eruption. Further fracturing will occur during the eruption. This process will then recur with timescales based on the rate of degassing and the strength of the seal. Following the rupture of the seal and the ensuing phreatic eruption, the system is likely to remain open for a period of time until hydrothermal deposition begins to close the system anew.

5. Conclusions

Since its reactivation, Turrialba has experienced frequent phreatic eruptions which are unpredictable and dangerous by nature. We propose that these eruptions are the result of hydrothermal sealing wherein the fluids circulating within the shallow magmatic-hydrothermal system first leach the rocks, then deposit hydrothermal minerals, resulting in a loss of permeability leading to sealing and gas accumulation. Sufficient gas accumulation will in time result in overpressure and eventual failure of the seal triggering eruptions.

A suite of pyroclastic breccias believed to be pieces of failed seals that resulted in phreatic eruptions between 2014 and 2019 have been analyzed for their mineralogy and physical properties. An alteration assemblage of SiO_2 polymorphs ± gypsum ± natroalunite ± pyrite was identified for all samples, indicative of acid sulphate alteration within the advanced argillic alteration facies. This alteration is consistent with fluids of pH <4 and of 200–350 °C. The alteration mineralogy is present within the ash matrix, as replacement of primary igneous minerals, and filling fractures. Given that sealing would result in a loss of permeability,

samples were analyzed for both gas and liquid permeability (Christenson et al., 2010). Gas permeability varied from <0.001 mD to 10.6 mD while permeability values for liquids varied from <0.001 mD to 7.68 mD. Compared to fresh analogues from White Island, New Zealand, analyzed by Heap et al. (2017) with permeabilities of 1.80–11.25 mD, all samples display a decrease in permeability associated with alteration. This decrease is principally due to infilling of a network of fractures displaying a high degree of connectivity, the fractures consisting of an interconnected network of macro-scale fractures, micro-fractures, and nano-fractures.

The repeated eruptions at Turrialba between 2014 and 2019 suggest that sealing can be a recurring process at relatively short timescales. We propose that sealing will continue to result in phreatic eruptions at Turrialba as long as the magmatic-hydrothermal system remains in its current state with magmatic gases supplied by the crystallizing magma below. Additionally, hydrothermal sealing occurs by degrees, so a complete seal is not necessary in order for phreatic eruptions to be triggered. The presence of a near-continuous plume of gas present at Turrialba since 2014 indicates that sealing is partial (de Moor et al., 2016a). Given the knowledge that hydrothermal sealing is an ongoing and recurring process at Turrialba, continuous real-time monitoring may provide insight into seal rupturing and improve the early detection of these eruptions.

CRediT authorship contribution statement

Emily Mick: Conceptualization, Methodology, Investigation, Writing - original draft, Visualization. **John Stix**: Conceptualization, Methodology, Resources, Writing - review & editing, Supervision. **J. Maarten de Moor**: Resources, Writing - review & editing. **Geoffroy Avard**: Resources, Writing - review & editing.

Declaration of Competing Interest

The authors declare that they have no known competing financial interests or personal relationships that could have appeared to influence the work reported in this paper.

Acknowledgements

The authors would like to thank Felix-Antoine Comeau and Jasmin Raymond of INRS Quebec City for their assistance with the collection of physical properties data as well as Christie Rowe and Lang Shi for their assistance with XRD and SEM analysis respectively. The authors would also like to thank Hans Larson and Rui Tahara from the McGill Cell Imaging and Analysis Network for sharing their expertise in CT-scanning. Lastly, the authors would like to thank James Gardner and Maurizio Battaglia whose reviews allowed us to improve both the science and presentation of this paper. This work was supported by Discovery grants to JS from the Natural Sciences and Engineering Research Council of Canada, and funding to JMdM and GA for volcano monitoring from Costa Rica National Law for Emergencies and Risk Prevention No. 8488 Transitorio I.

Appendix A. Supplementary data

Supplementary data to this article can be found online at https://doi.org/10.1016/j.jvolgeores.2021.107297.

References

Alvarado, G.E., 2009. Los Volcanes de Costa Rica: Geología, Historia, Riqueza Natural y du Gente. 3rd ed. Editorial Universidad Estatal a Distancia, San José, Costa Rica.

Alvarado, G.E., Mele, D., Dellino, P., de Moor, J.M., Avard, G., 2016. Are the ashes from the latest eruptions (2010–2016) at Turrialba volcano (Costa Rica) related to phreatic or phreatomagmatic events? J. Volcanol. Geotherm. Res. 327, 407–415. https://doi.org/10.1016/j.jvolgeores.2016.09.003.

Armstrong, D.C., 1995. Acid sulphate alteration in a magmatic hydrothermal environment, Barton Peninsula, King George Island, Antarctica. Mineral. Mag. 59, 429–441. https://doi.org/10.1180/minmag.1995.059.396.05.

Barberi, F., Bertagnini, A., Landi, P., Principe, C., 1992. A review on phreatic eruptions and their precursors. J. Volcanol. Geotherm. Res. 52, 231–246. https://doi.org/10.1016/0377-0273(92)90046-G.

Barton, C.C., Hsieh, P.A., 1989. Physical and Hydrologic-flow Properties of Fractures: Las Vegas, Nevada - Zion Canyon, Utah - Grand Canyon, Arizona - Yucca Mountain, Nevada, July 20–24, 1989, Field Trip Guidebook. American Geophysical Union, Washington, DC.

Campion, R., Martinez-Cruz, M., Lecocq, T., Caudron, C., Pacheco, J., Pinardi, G., Hermans, C., Carn, S., Bernard, A., 2012. Space- and ground-based measurements of sulphur dioxide emissions from Turrialba Volcano (Costa Rica). Bull. Volcanol. 74, 1757–1770. https://doi.org/10.1007/s00445-012-0631-z.

Christenson, B.W., Tassi, F., 2015. Gases in volcanic lake environments. In: Rouwet, D., Christenson, B., Tassi, F., Vandemeulebrouck, J. (Eds.), Volcanic Lakes,Advances in Volcanology. Springer Berlin Heidelberg, Berlin, pp. 125–153 https://doi.org/10.1007/978-3-642-36833-2_5.

Christenson, B.W., Wood, C.P., 1993. Evolution of a vent-hosted hydrothermal system beneath Ruapehu Crater Lake, New Zealand. Bull. Volcanol. 55, 547–565. https://doi.org/10.1007/BF00301808.

Christenson, B.W., Reyes, A.G., Young, R., Moebis, A., Sherburn, S., Cole-Baker, J., Britten, K., 2010. Cyclic processes and factors leading to phreatic eruption events: Insights from the 25 September 2007 eruption through Ruapehu Crater Lake, New Zealand. J. Volcanol. Geotherm. Res. 191, 15–32. https://doi.org/10.1016/j.jvolgeores.2010.01.008.

de Moor, J.M., Aiuppa, A., Avard, G., Wehrmann, H., Dunbar, N., Muller, C., Tamburello, G., Giudice, G., Liuzzo, M., Moretti, R., Conde, V., Galle, B., 2016a. Turmoil at Turrialba Volcano (Costa Rica): degassing and eruptive processes inferred from high-frequency gas monitoring. J. Geophys. Res. 121, 5761–5775. https://doi.org/10.1002/2016JB013150.

de Moor, J.M., Aiuppa, A., Pacheco, J., Avard, G., Kern, C., Liuzzo, M., Martínez, M., Giudice, G., Fischer, T.P., 2016b. Short-period volcanic gas precursors to phreatic eruptions: insights from Poás Volcano, Costa Rica. Earth Planet. Sci. Lett. 442, 218–227. https://doi.org/10.1016/j.epsl.2016.02.056.

de Moor, J.M., Muller, C., Pacheco, J., Mora, M., Avard, G., Aiuppa, A., Alvarado, G., Kern, C., Kelly, P., Pesicek, J., Wright, H., Pallister, J., Marso, J., 2017. The Slow Awakening of Turrialba Volcano: An Increasing Challenge for Eruption Forecasts, IAVCEI 2017. Portland, Oregon.

Di Piazza, A., Rizzo, A.L., Barberi, F., Carapezza, M.L., De Astis, G., Romano, C., Sortino, F., 2015. Geochemistry of the mantle source and magma feeding system beneath Turrialba volcano, Costa Rica. Lithos 232, 319–335. https://doi.org/10.1016/j.lithos.2015.07.012.

Farquharson, J.I., Wild, B., Kushnir, A.R.L., Heap, M.J., Baud, P., Kennedy, B., 2019. Acid-induced dissolution of andesite: evolution of permeability and strength. J. Geophys. Res. 124, 257–273. https://doi.org/10.1029/2018JB016130.

Fuller, C.M., Sharp, J.M., 1992. Permeability and fracture patterns in extrusive volcanic rocks: implications from the welded Santana Tuff, Trans-Pecos Texas. GSA Bull. 1992 (104), 1485–1496. https://doi.org/10.1130/0016-7606(1992)104<1485:PAFPIE;/;2.3.CO;2.

Global Volcanism Program, 2012. Report on Turrialba, Costa Rica. In: Wunderman, R. (Ed.), Bulletin of the Global Volcanism Network, 37:6. Smithsonian Institute https://doi.org/10.5479/si.GVP.BGVN201206-345070.

Global Volcanism Program, 2015. Report on Turrialba, Costa Rica. In: Wunderman, R. (Ed.), Bulletin of the Global Volcanism Network, 40:4. Smithsonian Institute. https://doi.org/10.5479/si.GVP.BGVN201206-345070.

Global Volcanism Program, 2017. Report on Turrialba, Costa Rica. In: Crafford, A.E., Venske, E. (Eds.), Bulletin of the Global Volcanism Network, 42:6. Smithsonian Institute https://doi.org/10.5479/si.GVP.BGVN201706-345070.

Global Volcanism Program, 2018. Report on Turrialba, Costa Rica. In: Venske, E. (Ed.), Bulletin of the Global Volcanism Network, 43:9. Smithsonian Institute https://doi.org/10.5479/si.GVP.BGVN201809-345070.

Global Volcanism Program, 2019a. Report on Turrialba, Costa Rica. In: Venske, E. (Ed.), Bulletin of the Global Volcanism Network, 44:4. Smithsonian Institute https://doi.org/10.5479/si.GVP.BGVN201904-345070.

Global Volcanism Program, 2019b. Report on Turrialba, Costa Rica. In: Venske, E. (Ed.), Bulletin of the Global Volcanism Network, 44:11. Smithsonian Institute https://doi.org/10.5479/si.GVP.BGVN201809-345070.

Heap, M.J., Kennedy, B.M., 2016. Exploring the scale-dependent permeability of fractured andesite. Earth Planet. Sci. Lett. 447, 139–150. https://doi.org/10.1016/j.epsl.2016.05.004.

Heap, M.J., Kennedy, B.M., Farquharson, J.I., Ashworth, J., Mayer, K., Letham-Brake, M., Reuschlé, T., Gilg, H.A., Scheu, B., Lavallée, Y., Siratovich, P., Cole, J., Jolly, A.D., Baud, P., Dingwell, D.B., 2017. A multidisciplinary approach to quantify the permeability of the Whakaari/White Island volcanic hydrothermal system (Taupo Volcanic Zone, New Zealand). J. Volcanol. Geotherm. Res. 332, 88–108. https://doi.org/10.1016/j.jvolgeores.2016.12.004.

Heap, M.J., Troll, V.R., Kushnir, A.R.L., Gilg, H.A., Collinson, A.S.D., Deegan, F.M., Darmawan, H., Seraphine, N., Neuberg, J., Walter, T.R., 2019. Hydrothermal alteration of andesitic lava domes can lead to explosive volcanic behaviour. Nat. Commun. 10, 5063. https://doi.org/10.1038/s41467-019-13102-8.

Henley, R.W., Berger, B.R., 2011. Magmatic-vapor expansion and the formation of high-sulfidation gold deposits: chemical controls on alteration and mineralization. Ore Geol. Rev. 39, 63–74. https://doi.org/10.1016/j.oregeorev.2010.11.003.

Ikehata, K., Maruoka, T., 2016. Sulfur isotopic characteristics of volcanic products from the September 2014 Mount Ontake eruption, Japan. Earth Planets Space 68, 116. https://doi.org/10.1186/s40623-016-0496-z.
John, D.A., Sisson, T.W., Breit, G.N., Rye, R.O., Vallance, J.W., 2008. Characteristics, extent and origin of hydrothermal alteration at Mount Rainier Volcano, Cascades Arc, USA: implications for debris-flow hazards and mineral deposits. J. Volcanol. Geotherm. Res. 175, 289–314. https://doi.org/10.1016/j.jvolgeores.2008.04.004.
Kaneko, T., Maeno, F., Nakada, S., 2016. 2014 Mount Ontake eruption: characteristics of the phreatic eruption as inferred from aerial observations. Earth Planets Space 68, 72. https://doi.org/10.1186/s40623-016-0452-y.
Kato, A., Terakawa, T., Yamanaka, Y., Maeda, Y., Horikawa, S., Matsuhiro, K., Okuda, T., 2015. Preparatory and precursory processes leading up to the 2014 phreatic eruption of Mount Ontake, Japan. Earth Planets Space 67, 111. https://doi.org/10.1186/s40623-015-0288-x.
Kilgour, G., Manville, V., Pasqua, F.D., Graettinger, A., Hodgson, K.A., Jolly, G.E., 2010. The 25 September 2007 eruption of Mount Ruapehu, New Zealand: directed ballistics, surtseyan jets, and ice-slurry lahars. J. Volcanol. Geotherm. Res. 191, 1–14. https://doi.org/10.1016/j.jvolgeores.2009.10.015.
Klimchouk, A., 1996. The dissolution and conversion of gypsum and anhydrite. Int. J. Speleol. 25, 21–36. https://doi.org/10.5038/1827-806X.25.3.2.
Marinelli, G., 1969. Some geological data on the geothermal areas of Tuscany. Bull. Volcanol. 33, 319–333. https://doi.org/10.1007/BF02596726.
Martini, F., Tassi, F., Vaselli, O., Del Potro, R., Martinez, M., del Laat, R.V., Fernandez, E., 2010. Geophysical, geochemical and geodetical signals of reawakening at Turrialba volcano (Costa Rica) after almost 150 years of quiescence. J. Volcanol. Geotherm. Res. 198, 416–432. https://doi.org/10.1016/j.jvolgeores.2010.09.021.
Meyer, C., Hemley, J.J., 1967. Wall rock alteration at Butte, Montana. Am. Mineral. 50, 1717–1722.
Minami, Y., Imura, T., Hayashi, S., Ohba, T., 2016. Mineralogical study on volcanic ash of the eruption on September 27, 2014 at Ontake volcano, central Japan: correlation with porphyry copper systems. Earth Planets Space 68. https://doi.org/10.1186/s40623-016-0440-2.
Miyagi, I., Geshi, N., Hamasaki, S., Oikawa, T., Tomiya, A., 2020. Heat source of the 2014 phreatic eruption of Mount Ontake, Japan. Bull. Volcanol. 82, 33. https://doi.org/10.1007/s00445-020-1358-x.
Mordensky, S.P., Kennedy, B.M., Villeneuve, M.C., Lavallée, Y., Reichow, M.K., Wallace, P.A., Siratovich, P.A., Gravley, D.M., 2019. Increasing the permeability of hydrothermally altered andesite by transitory heating. Geochem. Geophys. Geosyst. 20, 5251–5269. https://doi.org/10.1029/2019GC008409.
Mordret, A., Jolly, A.D., Duputel, Z., Fournier, N., 2010. Monitoring of phreatic eruptions using interferometry on retrieved cross-correlation function from ambient seismic noise: results from Mt. Ruapehu, New Zealand. J. Volcanol. Geotherm. Res. 191, 46–59. https://doi.org/10.1016/j.jvolgeores.2010.01.010.
Mori, T., Hashimoto, T., Terada, A., Yoshimoto, M., Kazahaya, R., Shinohara, H., Tanaka, R., 2016. Volcanic plume measurements using a UAV for the 2014 Mt.Ontake eruption. Earth Planets Space 68, 49. https://doi.org/10.1186/s40623-016-0418-0.
Oikawa, T., Yoshimoto, M., Nakada, S., Maeno, F., Komori, J., Shimano, T., Takeshita, Y., Ishizuka, Y., Ishimine, Y., 2016. Reconstruction of the 2014 eruption sequence of Ontake Volcano from recorded images and interviews. Earth Planets Space 68, 79. https://doi.org/10.1186/s40623-016-0458-5.
Reagan, M., Duarte, E., Soto, G.J., Fernández, E., 2006. The eruptive history of Turrialba volcano, Costa Rica, and potential hazards from future eruptions. In: Rose, W.I., Bluth, G.J.S., Carr, M.J., Ewert, J.W., Patino, L.C., Vallance, J.W. (Eds.), Volcanic Hazards in Central America. 412. Geological Society of America Special Paper, pp. 235–257. https://doi.org/10.1130/2006.2412(13).
Rizzo, A.L., Piazza, A.D., de Moor, J.M., Alvarado, G.E., Avard, G., Carapezza, M.L., Mora, M.M., 2016. Eruptive activity at Turrialba volcano (Costa Rica): inferences from 3He/4He in fumarole gases and chemistry of the products ejected during 2014 and 2015. Geochem. Geophys. Geosyst. 17, 4478–4494. https://doi.org/10.1002/2016GC006525.
Rodriguez, A., van Bergen, M.J., 2017. Superficial alteration mineralogy in active volcanic systems: an example of Poás volcano, Costa Rica. J. Volcanol. Geotherm. Res. 346, 54–80. https://doi.org/10.1016/j.jvolgeores.2017.04.006.
Soto, G., 1988. Estructuras volcano-tectónicas del volcán Turrialba, Costa Rica, América Central. Actas Quinto Congreso Geológico Chileno, Santiago, Chile, pp. 163–175.
Stix, J., de Moor, J.M., 2018. Understanding and forecasting phreatic eruptions driven by magmatic degassing. Earth Planets Space 70, 1–19. https://doi.org/10.1186/s40623-018-0855-z.
Stoffregen, R.E., 1987. Genesis of acid-sulfate alteration and Au-Cu-Ag mineralization at Summitville, Colorado. Econ. Geol. 82, 1575–1591. https://doi.org/10.2113/gsecongeo.82.6.1575.
Stoffregen, R.E., Alpers, C.N., Jambor, J.L., 2000. Alunite-Jarosite crystallography, thermodynamics, and geochronology. Rev. Mineral. Geochem. 40, 453–479. https://doi.org/10.2138/rmg.2000.40.9.
Vaselli, O., Tassi, F., Duarte, E., Fernandez, E., Poreda, R.J., Huertas, A.D., 2010. Evolution of fluid geochemistry at the Turrialba volcano (Costa Rica) from 1998 to 2008. Bull. Volcanol. 72, 397–410. https://doi.org/10.1007/s00445-009-0332-4.
Whattam, S.A., Stern, R.J., 2016. Arc magmatic evolution and the construction of continental crust at the Central American Volcanic Arc system. Int. Geol. Rev. 58, 653–686. https://doi.org/10.1080/00206814.2015.1103668.
Zimbelman, D.R., Rye, R.O., Breit, G.N., 2005. Origin of secondary sulfate minerals on active andesitic stratovolcanoes. Chem. Geol. 215, 37–60. https://doi.org/10.1016/j.chemgeo.2004.06.056.